Spin and electronic correlations in gated graphene quantum rings

P. Potasz,[1,2] A. D. Güçlü,[1] and P. Hawrylak[1]
[1]*Institute for Microstructural Sciences, National Research Council of Canada, Ottawa, Canada*
[2]*Institute of Physics, Wroclaw University of Technology, Wroclaw, Poland*
(Received 26 May 2010; published 25 August 2010)

We present a theory of graphene quantum rings designed to produce degenerate shells of single-particle states close to the Fermi level. We show that populating these shells with carriers using a gate leads to correlated ground states with finite total electronic spin. Using a combination of tight-binding and configuration-interaction methods, we predict the ground state and the total spin of the system as a function of the filling of the shell. We show that for smaller quantum rings, the spin polarization of the ground state at half filling depends strongly on the size of the system but reaches a maximum value beyond a critical size.

DOI: 10.1103/PhysRevB.82.075425 PACS number(s): 75.75.−c, 31.15.V−

I. INTRODUCTION

There is currently significant interest in developing understanding of electronic properties[1–6] and applications[6–8] of graphene. Starting with graphene as a zero-gap nonmagnetic material, reducing the lateral size and controlling the shape and the character of the edges opens the possibility of controlling the energy spectrum and hence electronic and magnetic properties of graphene nanostructures.[9–15] In particular, the zigzag edges are responsible for degenerate energy shells at the Fermi level,[14–23] and associated finite spin polarization as a result of electron-electron exchange interactions.[16–24] However, the coupling of spin-polarized zigzag edges was shown to be antiferromagnetic in graphene nanoribbons[16] with no net spin polarization. In contrast, in triangular graphene quantum dots spin-polarized edges were shown to couple ferromagnetically leading to a finite magnetic moment.[20–22,24] The purpose of this work is to answer the question whether it is possible to use graphene nanoribbons to build graphene nanostructures with finite magnetic moment. We show here that by designing a hexagonal ring from six ribbons we obtain a quantum system with degenerate shells in the energy spectrum. By filling these shells with additional electrons using metallic gate, we obtain maximally spin-polarized ground state for the half filling of the degenerate shell.

Semiconductor quantum rings have been investigated by a number of groups.[25–28] The ring geometry allows to observe quantum phenomena, e.g., persistent current and quantum interference effects,[29] in particular, Aharonov-Bohm (AB) oscillations.[25] The AB oscillations manifest themselves as periodic oscillations in the energy spectrum of the electronic system as a function of the number of flux quanta entering the ring.[26] The AB effect for a single electron in single lithographically defined semiconductor quantum ring,[27] hole in a type-II semiconductor dot[28] and exciton[30,31] in a finite ring, was demonstrated.

The AB conductance oscillations were also recently observed in a graphene ring.[32,33] The electronic properties of a single Dirac Fermion in graphene quantum rings were studied using effective mass[34,35] and tight-binding (TB) methods.[34,36,37] Valley degeneracy in graphene was shown to be lifted by the magnetic field[34,36] since the magnetic field has the opposite sign in the two valleys. The AB effect was also studied in Refs. 13 and 38.

In this work, we combine the tight-binding method with the configuration-interaction method to determine the electronic and spin properties of graphene quantum rings with zigzag edges as a function of the number of additional electrons controlled by the gate. We analyze the energy spectrum of quantum rings as a function of the width of the ring and its size. We find degenerate electronic shells near Fermi energy for the thinnest structures. We use the configuration-interaction method to treat exactly interaction of additional electrons in the degenerate shell as a function of shell filling. We determine the dependence of the spin polarization of the ground state on the filling of the degenerate shell and the size of the structure. We show that by changing the size of the structures, we control the splitting between levels in a degenerate shell which in turn significantly influences magnetic properties of the ground state. The stabilization of the spin phase diagram at a critical size of the ring is observed.

This paper is organized as follows. In Sec. II, we introduce both the TB model for single-particle levels and the configuration-interaction method for electron-electron interaction. In Sec. III, in order to explain the single-particle spectrum, we show the method for constructing hexagonal ring structures with different width and length. Next, in Sec. IV we present discussion of single-particle energy spectra and show the origin of the shell structure. In Sec. V, we analyze the effect of electron-electron interactions and spin properties of electrons in degenerate shells as a function of shell filling. Finally, in Sec. VI, we summarize obtained results.

II. MODEL AND METHOD

The single-particle energy spectrum of π_z electrons in graphene quantum rings can be obtained using the tight-binding Hamiltonian.[39] The tight-binding model was successfully applied to carbon materials such as graphite, graphene, nanoribbons, nanotubes, fullerenes, and graphene quantum dots.[14,15,17–20,39] The Hamiltonian in the nearest neighbors' approximation can be written as

$$H = t \sum_{\langle i,j\rangle,\sigma} c_{i\sigma}^{\dagger} c_{j\sigma}, \tag{1}$$

where t is the hopping integral, $c_{i\sigma}^{\dagger}$ and $c_{i\sigma}$ are creation and annihilation operators of electron on π_z orbital on site i with spin $\sigma=\uparrow,\downarrow$, respectively, and $\langle i,j\rangle$ indicate summation over nearest neighbors. Diagonalization of the tight-binding Hamiltonian generates single-particle energies ϵ_s and single-particle orbitals $|s,\sigma\rangle$.

In order to include electron-electron interactions, the many-body Hamiltonian H_{MB} is written as

$$H_{MB} = \sum_{s,\sigma} \epsilon_s a_{s\sigma}^{\dagger} a_{s\sigma} + \frac{1}{2} \sum_{\substack{s,p,d,f,\\ \sigma,\sigma'}} \langle sp|\tilde{V}|df\rangle a_{s\sigma}^{\dagger} a_{p\sigma'}^{\dagger} a_{d\sigma'} a_{f\sigma}, \tag{2}$$

where the first term describes single-particle energies obtained from the tight-binding Hamiltonian given by Eq. (1) and the second term describes interactions between particles occupying these single-particle states. By using Slater π_z orbitals,[40] we calculated two-body Coulomb matrix elements $\langle ij|V|kl\rangle$, where i, j, k, l are the site indices [see also Eqs. (A1)–(A3) in the Appendix]. In numerical calculations, on-site and all scattering and exchange terms up to next-nearest neighbors are included. Few largest Coulomb matrix elements are given in the Appendix. We use $t=-2.5$ eV for the hopping integral. The hopping integral is a fitting parameter usually residing between −2 and −3 eV, depending on the experimental data[41] or *ab initio* calculation.[42] The value of the effective dielectric constant κ depends on the substrate, and is set to $\kappa=6$, in what follows.[41] The Hamiltonian given by Eq. (2) is diagonalized in the basis of all possible configurations of electrons distributed within single-particle states (the configuration-interaction method). Since the total spin of the system is conserved, the Hamiltonian has block-diagonal form in subspaces with projection of total spin onto z-axis S_z.

III. CONSTRUCTION OF GRAPHENE RINGS

In order to understand the origin of single-particle spectrum of the ring, we first consider six independent nanoribbons, then bring them together by turning on the hopping between the connecting atoms. In Fig. 1, we show two sets of six graphene ribbons arranged in a hexagonal ring. Each ribbon consists of two types of atoms from the unit cell of honeycomb lattice, indicated by red (light gray) and blue (dark gray) circles in Fig. 1. On the left side, thinnest possible ribbons with one benzene ring width are shown, denoted as $W=1$. Each of them consists of 16 atoms. The length $L=4$, is measured by the number of one type of atoms in the upper row so the final ring is built of 96 atoms. Small black arrows in the bottom enlargement indicate bonds and hopping integrals between nearest neighbors in a tight-binding model between neighboring ribbons, two arrows in the case of thinnest structures. The number of such connecting atoms increases with increasing width as seen on the right hand side of Fig. 1. The thicker ribbon $W=2$ has identical length to the one from the left side $L=4$. In this case, there are three connecting atoms. Three small black arrows in the bottom enlargement indicate three bonds. The final ring is built of 126 atoms. By connecting neighboring ribbons with different lengths and widths, we create rings with different single-particle spectra.

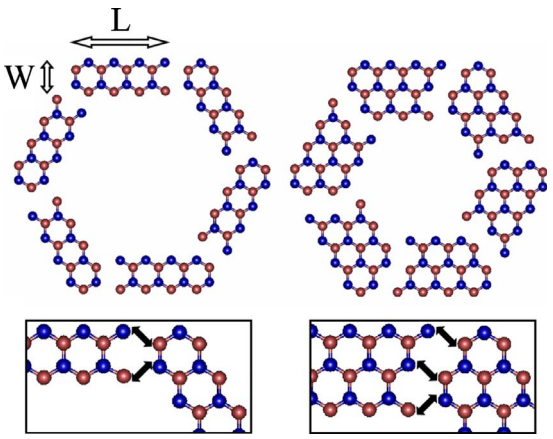

FIG. 1. (Color online) Construction of ring structures from six ribbonlike units. On the left, there are six thinnest possible ribbons (one benzene ring thick denoted as $W=1$) arranged in a hexagonal ring structure. The length of each ribbon is given by $L=4$, the number of one type of atoms in one row. Each ribbon consists of 16 atoms which gives a total of 96 atoms in a ring. On the right, there are six ribbons with width $W=2$ (two benzene ring thick). Each of them consists of 21 atoms giving a total of 126 atoms in a ring. We create a thicker ring with similar length $L=4$ but smaller antidot inside. Small black arrows in the bottom enlargement indicate bonds and hopping integrals between nearest neighbors in a tight-binding model between neighboring ribbons.

IV. SINGLE-PARTICLE SPECTRA

In Fig. 2, we show the single-particle energy levels near Fermi level obtained by diagonalizing tight-binding Hamiltonian, Eq. (1), for rings with length $L=8$ and different

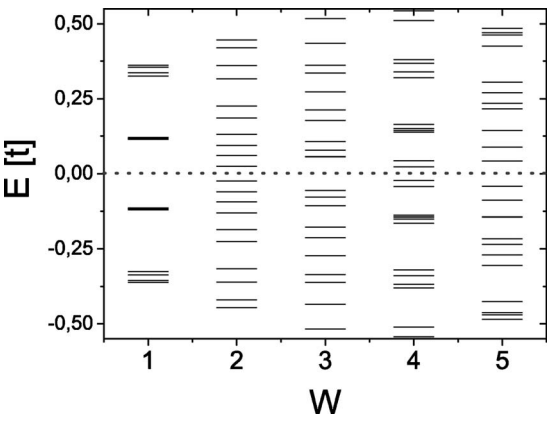

FIG. 2. Single-particle spectrum near Fermi level for ring structures with $L=8$, different widths W and $t'=t$ (see Fig. 3). The shell structure is clearly observed only for the thinnest ring $W=1$. Dotted line indicates the location of Fermi energy.

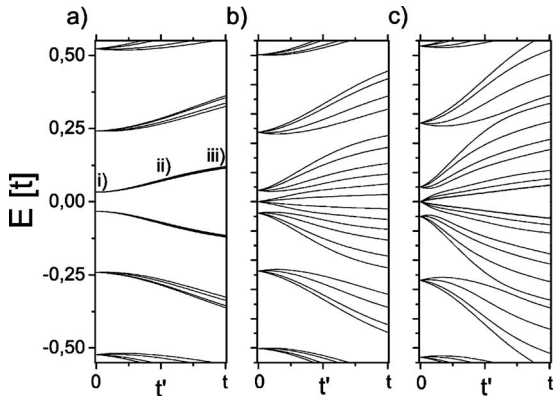

FIG. 3. The evolution of the single-particle spectrum from six independent ribbons with $L=8$ to a hexagonal ring structure spectrum. t' indicate hopping integrals between neighboring ribbons. (a) For the thinnest ring $W=1$, sixfold degeneracy is slightly removed, preserving a shell structure. For thicker structures [(b) and (c), $W=2$ and $W=3$, respectively] the sixfold degeneracy is strongly lifted and shell structure is not observed.

widths W. The thinnest ring $W=1$ consists of 192 atoms. For this structure, we observe nearly degenerate shells of energy levels separated by gaps. Each shell consists of six levels: two single and two doubly degenerate states. The first shell over the Fermi level is almost completely degenerate while in the second one, the degeneracy is slightly removed. We note that for rings with different lengths, the gap between the first and second shell is always larger then the gap at the Fermi level. With increasing width of the ring, the spectrum changes completely. For the rings with width $W=2$ (270 atoms), $W=3$ (336 atoms), and $W=5$ (432 atoms), shells are not visible. For $W=4$ (390 atoms), we observe appearance of shells separated by gaps further from Fermi level but the splitting between levels in these shells is much stronger in comparison to the thinnest ring. We note that for $W\geq 2$, although we do not observe a clear pattern of shells around the Fermi level, single shells of six levels separated by gaps from the rest of the spectrum appear far away from the Fermi energy in some cases.

In order to have a better understanding of the structure of the tight-binding spectra, in Fig. 3 we show the evolution of single-particle energies from six independent ribbons to a ring as the hopping t' between the ribbons is increased. To achieve this, we first diagonalize the tight-binding Hamiltonian matrix for a single ribbon. We then take six such ribbons and create Hamiltonian matrix in the basis of the eigenvectors of six ribbons. Here, the matrix has diagonal form. All energy levels are at least sixfold degenerate. Next, using the six ribbons basis, we write hopping integrals corresponding to connecting atoms between neighboring ribbons indicated by small black arrows in Fig. 1. By slowly turning on the hopping integrals and diagonalizing the Hamiltonian at every step, we can observe the evolution of the spectrum from single-particle states of six independent ribbons to a ring.

The hopping integrals between connecting atoms of neighboring ribbons are indicated by t' in Fig. 3. For the thinnest ring [Fig. 3(a)], each ribbon consists of 32 atoms. There are only two connecting atoms between neighboring ribbons, giving only two hopping integrals t' between each two ribbons in the nearest neighbors' approximation. We see that their influence is very small and sixfold degenerate states evolve into shells with a very small splitting between levels. We note that this splitting is a bit stronger for higher energy levels but due to large gaps between consecutive levels of single ribbon the shell structure is still clearly observed. For the thicker structures [Figs. 3(b) and 3(c)], the evolution of the spectrum has a more complicated behavior. For a given ring, each ribbon consists of different number of two types of atoms giving rise to zero-energy edge states.[43] With increasing width, the number of zero-energy states increases as well as the number of connecting atoms and equally the number of t' hopping integrals (see enlaregement in Fig. 1). This causes a stronger splitting of levels for thicker rings in comparison to the thinnest one. Thus, the thicker ring's spectrum close to the Fermi level is due to the splitting of zero-energy states of independent ribbons. For $W=2$ (one zero-energy state) and $W=3$ (two zero-energy states), each ribbon consists of 45 and 56 atoms, respectively, and the evolution of their spectrum is similar. The degeneracy is strongly lifted and no shell structure is observed.

In order to illuminate the influence of t' hopping integrals on the thinnest ring spectrum, in Fig. 4 we also show the electronic densities for the first shell over the Fermi level for three different values of t' [indicated in Fig. 3(a)]. For $t'=0$, there are six independent ribbons and first shell is perfectly sixfold degenerate. The electronic charge density in each ribbon is larger on the two atoms with only one bond (see Fig. 1) and gradually decreases along the length. For $t'=0.5t$, the total energy of the shell increases and the degeneracy is slightly removed. Here, the highest peak of the electronic charge density is moved toward the center of each ribbon in comparison to $t'=0$ case. Increasing t' to t causes increase in the total energy of the shell and the highest peak of the electronic charge density is now perfectly in the middle of each arm of the ring. Thus, both the electronic charge density and the energy of levels change slightly during the gradual transition of ribbons into a hexagonal ring structure.

We find degenerate shells near the Fermi energy only for the thinnest rings $W=1$. In the rest of the paper, we will focus on the single- and many-particle properties of these structures as a function of their lengths. In Fig. 5, we show the low-energy spectrum for two thinnest rings with different lengths. We clearly see shells with six levels. The splitting of levels of the first shell over the Fermi level is smaller for larger ring. For ring structure with $L=4$, the difference between the highest and the lowest energy of levels forming the first shell is around $0.069t\approx 0.17$ eV. In comparison, for ring with $L=8$ this value is around $0.006t\approx 0.015$ eV. Thus, we conclude that for smaller rings single-particle energies can play important role in the properties of many-particle states while for the larger rings, interactions are expected to be more important.

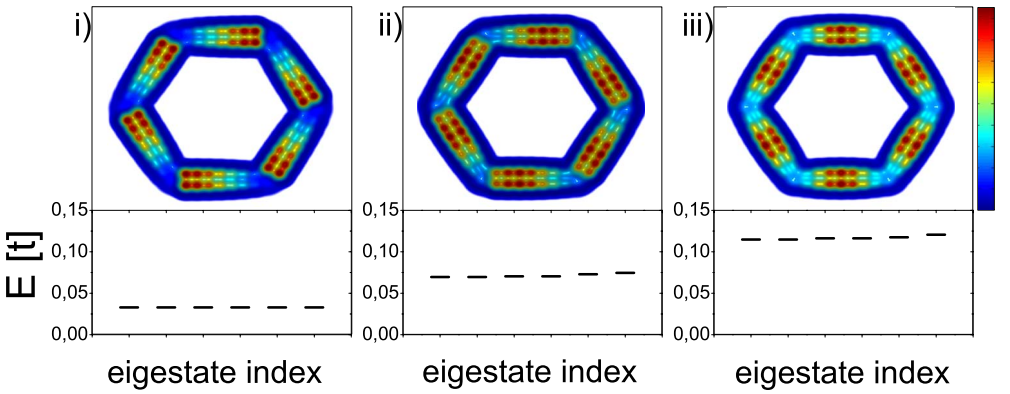

FIG. 4. (Color online) Energy levels and corresponding total electronic densities for the first six states over the Fermi level for the thinnest structure $W=1$ with $L=8$ (192 atoms), for (i) $t'=0$, (ii) $t'=0.5t$, and (iii) $t'=t$. The three values of t' hopping integrals are indicated in Fig. 3(a).

V. ELECTRONIC INTERACTIONS IN A DEGENERATE ELECTRONIC SHELL OF A GRAPHENE QUANTUM RING

In this section, we study the ground and excited states as a function of the number of additional interacting electrons in degenerate shells of quantum rings with different size L and $W=1$. In our calculations, we assume that all states below the Fermi level remain fully occupied. This is justified as long as there is a sufficiently large energy gap at the Fermi level. Next, we add extra electrons to the charge-neutral system. In a first approximation, we neglect scatterings from/to the states below the Fermi energy. Moreover, because of the large energy gap between the first and second shell we can neglect scatterings to the higher energy states. Our assumptions can be confirmed by comparing the energy gaps and Coulomb interaction matrix elements. For the ring with $L=8$ and $W=1$, both gaps $\Delta E \sim 0.5$ eV while the intrashell interaction terms $V \sim 0.23$ eV. The Coulomb matrix elements V scattering electrons from the first shell to valence band and/or to second shell are $V \sim 0.2$ eV. Hence, the effect of scattering to other shells, proportional to $V^2/\Delta E \ll 1$, is weak. Thus, many-body properties of electrons occupying a shell are primarily governed by interactions between electrons within a shell. This allows us to treat first shell over the Fermi level of the thinnest ring as an independent system which significantly reduces the dimension of the Hilbert space. All the shells in the studied structures consist of six levels. The largest dimension of the Hilbert subspace is for the half filling, six electrons, $S_z=0$ for which there are 400 configurations (see description of the method in Sec. II).

First, we study total spin of the half-filled shell. Figure 6 shows the low-energy spectra for the different total spin S of half-filled first shell over the Fermi energy for two thinnest rings with (a) $L=4$ (96 atoms) and (b) $L=8$ (192 atoms). For smaller ring, the ground state has total spin $S=1$ with a very small gap to the first excited state with $S=0$.[38] The lowest

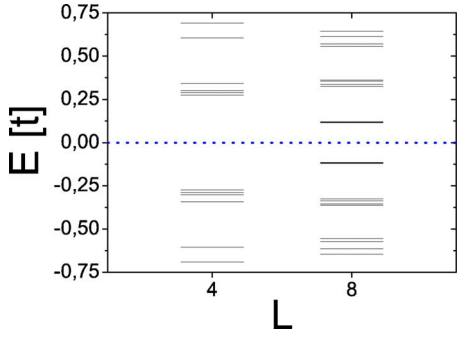

FIG. 5. (Color online) Single-particle spectrum near Fermi level for the thinnest ring structures $W=1$ with length $L=8$ and $L=4$. The shell structure is clearly observed. The splitting between levels in the first shell is smaller for larger structure. Dotted blue (gray) line indicate the location of Fermi energy.

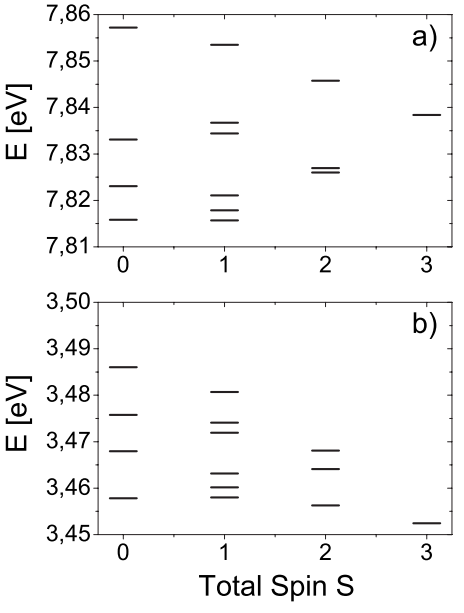

FIG. 6. The low-energy spectra for the different total spin S of half-filled first shell over the Fermi energy for two thinnest rings $W=1$ with (a) $L=4$ (96 atoms) and (b) $L=8$ (192 atoms).

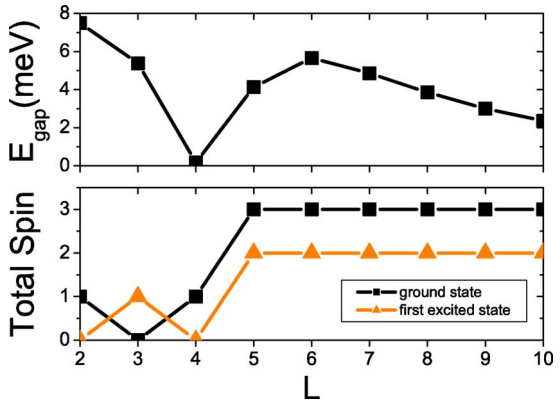

FIG. 7. (Color online) Lower: total spin of the ground and first excited states for the half filling of the first shell in the thinnest ring structures $W=1$ with different sizes. Upper: corresponding energy spin gap between ground and first excited states.

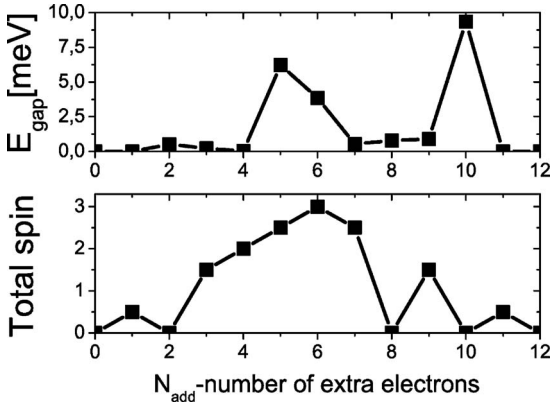

FIG. 8. Lower: the spin phase diagram for electrons occupying the first shell over the Fermi level of the ring structure with $L=8$ (192 atoms). Upper: corresponding energy spin gap between ground and first excited states.

states with larger total spin have higher energies. For 192 atoms ring, the total spin of the ground state is maximal, $S=3$. The lowest levels with different total spin have slightly higher energies. This can be understood in a following way. The splitting between levels is large for smaller structures, which is seen in Fig. 5. For ring with $L=4$ (96 atoms), this value, 0.17 eV, is comparable with electronic interaction terms, e.g., 0.34 eV for two electrons occupying the lowest state. For ring with $L=8$ (192 atoms), the electron-electron interaction terms are 0.23 eV for interaction between two particles on the first state, which is much larger then single-particle energy difference 0.015 eV. From this, we clearly see that for ring with $L=4$, it is energetically favorable to occupy low-energy states by electrons with opposite spins. For ring with $L=8$, all states have similar energies and due to exchange interactions the lowest-energy state is maximally spin polarized.

The behavior of magnetic properties of the ground state for half-filled shell as a function of size is shown in Fig. 7. In this case, the ground-state spin can be explained as a result of the competition between occupation of levels with smallest single-particle energies which favors opposite spin configurations, and parallel spin configurations for which exchange interactions are maximized. For rings with $L \geq 5$, the ground state is maximally spin polarized. Here, the splitting between levels is relatively small and the ground state is determined by electronic interactions. Moreover, this splitting decreases with increasing size and this is seen in the spin-gap behavior (Fig. 7). The largest spin gap is observed for ring with $L=6$ and decreases with increasing L. For small rings, the situation is more complicated. Here, the contributions from single-particle energies and interactions are comparable. As a consequence, we observe ground states with alternating total spin $S=1$ and $S=0$. For sufficiently large rings, $L>5$, we observe stabilization of the spin phase diagram. This is connected to changes in the energy differences between levels in a shell—above a critical size these values are so small that they do not play a role anymore.

In Fig. 8, we show the phase diagram for a ring with $L=8$ (192 atoms). Near the half filling, the ground state is maximally spin polarized which is related to the dominant contribution from the short-ranged exchange interaction terms, and charge density is symmetrically distributed in the entire ring (see Fig. 4). Adding or removing electrons causes irregularities in the density distribution, and correlation effects start becoming important. This results in an alternating spin between maximal polarization (e.g., three, four, and nine extra electrons) and complete depolarization (e.g., two, eight, and ten extra electrons) of the system.

VI. CONCLUSIONS

We presented here a theory of graphene quantum rings designed to produce degenerate shells of single-particle states close to the Fermi level. By combining tight-binding and configuration-interaction methods, we analyzed magnetic properties and electronic correlations in such structures as a function of size and number of added electrons. For the half filling of the degenerate shell in sufficiently large ring, maximal polarization of the ground state is predicted. Away from the half filling, the correlation effects appear and the ground-state total spin alternates between maximal polarization and complete depolarization. Preliminary results of this work were reported in Ref. 38.

ACKNOWLEDGMENTS

The authors thank NRC-CNRS CRP, Canadian Institute for Advanced Research, Institute for Microstructural Sciences, QuantumWorks, and Polish MNiSW, Grant No. N202-071-32/1513 for support.

APPENDIX: CALCULATIONS OF COULOMB MATRIX ELEMENTS

The Coulomb interaction term from Eq. (2),

$$V = \frac{1}{2} \sum_{\substack{s,p,d,f, \\ \sigma,\sigma'}} \langle sp|\tilde{V}|df\rangle a^{\dagger}_{s\sigma} a^{\dagger}_{p\sigma'} a_{d\sigma'} a_{f\sigma}$$

can be written in the basis of localized π_z orbitals as

$$V = \frac{1}{2} \sum_{\substack{s,p,d,f,\\ \sigma,\sigma'}} \left[\sum_{\substack{i,j,k,l,\\ \sigma,\sigma'}} \langle ij|V|kl\rangle A_i^s A_j^p A_k^d A_l^f c_{i\sigma}^\dagger c_{j\sigma'}^\dagger c_{k\sigma'} c_{l\sigma} \right], \tag{A1}$$

where we substituted $a_{s\sigma}=\Sigma_{i\sigma}A_i^s c_{i\sigma}$, and A_i^s are coefficients in transformation from localized to itinerant basis. Coulomb matrix elements in localized basis in atomic units (a.u.) for $\kappa=1$ are defined as

$$\langle ij|V|kl\rangle = \int\int d\mathbf{r}_1 d\mathbf{r}_2 \psi_i^*(\mathbf{r}_1)\psi_j^*(\mathbf{r}_2) \times \frac{1}{|\mathbf{r}_2-\mathbf{r}_1|}\psi_k(\mathbf{r}_2)\psi_l(\mathbf{r}_1), \tag{A2}$$

where 1 a.u.=27.211 eV and $\psi_i(\mathbf{r}_1)$ is Slater π_z orbital on a site i of electron 1, given by a function

$$\psi_i(\mathbf{r}_1) = \left(\frac{\xi^5}{32\pi}\right)^{1/2} z \exp\left(\frac{-\xi\mathbf{r}_1}{2}\right) \tag{A3}$$

with $\xi=3.14$.[40] In Table I, we show selected Coulomb matrix elements for $\kappa=1$. Numbers 1 and 2 and 3 indicate electron on-site and on nearest-neighbor site and on next-nearest-neighbor site of hexagonal lattice, respectively.

TABLE I. Selected coulomb matrix elements between electrons on sites in graphene honeycomb lattice for $\kappa=1$. Numbers 1, 2, and 3 indicate electron on-site, on nearest-neighbor site, and on next-nearest-neighbor site of hexagonal lattice, respectively.

$\langle ij\|V\|kl\rangle$	E (eV)
$\langle 11\|V\|11\rangle$	16.522
$\langle 12\|V\|21\rangle$	8.640
$\langle 13\|V\|31\rangle$	5.333
$\langle 11\|V\|12\rangle$	3.157
$\langle 12\|V\|31\rangle$	1.735
$\langle 12\|V\|12\rangle$	0.873
$\langle 11\|V\|22\rangle$	0.873
$\langle 22\|V\|13\rangle$	0.606

[1] K. S. Novoselov, A. K. Geim, S. V. Morozov, D. Jiang, Y. Zhang, S. V. Dubonos, I. V. Grigorieva, and A. A. Firsov, Science **306**, 666 (2004).
[2] K. S. Novoselov, A. K. Geim, S. V. Morozov, D. Jiang, M. I. Katsnelson, I. V. Grigorieva, S. V. Dubonos, and A. A. Firsov, Nature (London) **438**, 197 (2005).
[3] Y. B. Zhang, Y. W. Tan, H. L. Stormer, and P. Kim, Nature (London) **438**, 201 (2005).
[4] A. Rycerz, J. Tworzydlo, and C. W. Beenakker, Nat. Phys. **3**, 172 (2007).
[5] A. H. Castro Neto, F. Guinea, N. M. R. Peres, K. S. Novoselov, and A. K. Geim, Rev. Mod. Phys. **81**, 109 (2009).
[6] A. K. Geim and K. S. Novoselov, Nature Mater. **6**, 183 (2007).
[7] T. Mueller, F. Xia, and P. Avouris, Nat. Photonics **4**, 297 (2010).
[8] F. Xia, T. Mueller, Y.-M. Lin, A. Valdes-Garcia, and P. Avouris, Nat. Nanotechnol. **4**, 839 (2009).
[9] L. C. Campos, V. R. Manfrinato, J. D. Sanchez-Yamagishi, J. Kong, and P. Jarillo-Herrero, Nano Lett. **9**, 2600 (2009).
[10] J. Cai, P. Ruffieux, R. Jaafar, M. Bieri, T. Braun, S. Blankenburg, M. Muoth, A. P. Seitsonen, M. Saleh, X. Feng, K. Müllen, and R. Fasel, Nature (London) **466**, 470 (2010).
[11] H. P. Heiskanen, M. Manninen, and J. Akola, New J. Phys. **10**, 103015 (2008).
[12] Z. Z. Zhang, K. Chang, and F. M. Peeters, Phys. Rev. B **77**, 235411 (2008).
[13] D. A. Bahamon, A. L. C. Pereira, and P. A. Schulz, Phys. Rev. B **79**, 125414 (2009).
[14] M. Ezawa, Phys. Rev. B **73**, 045432 (2006).
[15] K. Nakada, M. Fujita, G. Dresselhaus, and M. S. Dresselhaus, Phys. Rev. B **54**, 17954 (1996).
[16] Y. Son, M. L. Cohen, and S. G. Louie, Nature (London) **444**, 347 (2006).
[17] T. Yamamoto, T. Noguchi, and K. Watanabe, Phys. Rev. B **74**, 121409 (2006).
[18] M. Ezawa, Phys. Rev. B **76**, 245415 (2007).
[19] M. Ezawa, Phys. Rev. B **77**, 155411 (2008).
[20] J. Fernández-Rossier and J. J. Palacios, Phys. Rev. Lett. **99**, 177204 (2007).
[21] A. D. Güçlü, P. Potasz, O. Voznyy, M. Korkusinski, and P. Hawrylak, Phys. Rev. Lett. **103**, 246805 (2009).
[22] W. L. Wang, S. Meng, and E. Kaxiras, Nano Lett. **8**, 241 (2008).
[23] B. Wunsch, T. Stauber, F. Sols, and F. Guinea, Phys. Rev. Lett. **101**, 036803 (2008).
[24] W. L. Wang, O. V. Yazyev, S. Meng, and E. Kaxiras, Phys. Rev. Lett. **102**, 157201 (2009).
[25] Y. Aharonov and D. Bohm, Phys. Rev. **115**, 485 (1959).
[26] R. A. Webb, S. Washburn, C. P. Umbach, and R. B. Laibowitz, Phys. Rev. Lett. **54**, 2696 (1985).
[27] M. Bayer, M. Korkusinski, P. Hawrylak, T. Gutbrod, M. Michel, and A. Forchel, Phys. Rev. Lett. **90**, 186801 (2003).
[28] E. Ribeiro, A. O. Govorov, W. Carvalho, Jr., and G. Medeiros-Ribeiro, Phys. Rev. Lett. **92**, 126402 (2004).
[29] M. Büttiker, Y. Imry, and R. Landauer, Phys. Lett. **96**, 365 (1983).
[30] R. A. Römer and M. E. Raikh, Phys. Rev. B **62**, 7045 (2000).
[31] M. D. Teodoro, V. L. Campo, Jr., V. Lopez-Richard, E. Marega, Jr., G. E. Marques, Y. G. Gobato, F. Iikawa, M. J. S. P. Brasil, Z. Y. AbuWaar, V. G. Dorogan, Yu. I. Mazur, M. Benamara, and G. J. Salamo, Phys. Rev. Lett. **104**, 086401 (2010).
[32] S. Russo, J. B. Oostinga, D. Wehenkel, H. B. Heersche, S. S. Sobhani, L. M. K. Vandersypen, and A. F. Morpurgo, Phys. Rev. B **77**, 085413 (2008).
[33] M. Huefner, F. Molitor, A. Jacobsen, A. Pioda, C. Stampfer, K. Ensslin, and T. Ihn, Phys. Status Solidi B **246**, 2756 (2009).
[34] P. Recher, B. Trauzettel, A. Rycerz, Ya. M. Blanter, C. W. J. Beenakker, and A. F. Morpurgo, Phys. Rev. B **76**, 235404 (2007).
[35] D. S. L. Abergel, V. M. Apalkov, and T. Chakraborty, Phys. Rev.

B **78**, 193405 (2008).
[36] J. Wurm, M. Wimmer, H. U. Baranger, and K. Richter, Semicond. Sci. Technol. **25**, 034003 (2010).
[37] P. H. Rivera, A. L. C. Pereira, and P. A. Schulz, Phys. Rev. B **79**, 205406 (2009).
[38] P. Potasz, A. D. Güçlü, and P. Hawrylak, Acta Phys. Pol. A **116**, 832 (2009).
[39] P. R. Wallace, Phys. Rev. **71**, 622 (1947).
[40] B. J. Ransil, Rev. Mod. Phys. **32**, 245 (1960).
[41] A. Bostwick, T. Ohta, J. L. McChesney, T. Seyller, K. Horn, and E. Rotenberg, Solid State Commun. **143**, 63 (2007).
[42] S. Reich, J. Maultzsch, C. Thomsen, and P. Ordejón, Phys. Rev. B **66**, 035412 (2002).
[43] E. H. Lieb, Phys. Rev. Lett. **62**, 1201 (1989).